CHIRALITY 2026

The 10th International Conference on Chirality, Vorticity and Magnetic Fields in Quantum Matter

Thermal Dileptons and ϕ/K^{*0} spin alignment in a hot Magnetized QCD matter

Xinyang Wang

Center for Fundamental Physics
Anhui University of Science and Technology (AUST)

Zhuhai, China / 16–20 November 2026

If you are interested in other projects from our group, see:

18 November Parallel Session 1

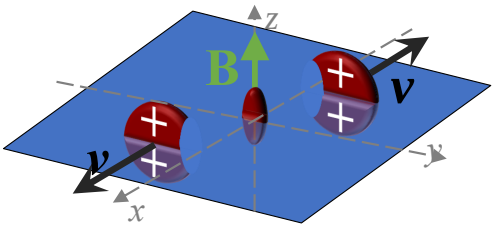
14:25–14:45 Zigeng Ding

Determining NJL Coupling Constants, Anomalous Magnetic Moments, and Meson Masses in Magnetized QCD Matter via Machine Learning

14:45–15:05 Zhaolu Ouyang

Drell-Yan process under an external magnetic field with full Landau levels

Magnetic field in HIC



- Moving spectator charges generate a strong magnetic field.
- The field introduces a preferred direction in the QGP.
- Electromagnetic emission and spin response can carry this anisotropy.

Magnetometer for HICs: how can we probe the field?

Our proposal: electromagnetic radiation as a magnetometer.

Our earlier picture: electromagnetic magnetometry

Magnetic fields change the emission mechanism

$$q \to q + \gamma, \qquad \bar{q} \to \bar{q} + \gamma, \qquad q + \bar{q} \to \gamma.$$

Landau quantization produces angular anisotropy already in a local equilibrium medium. The absorptive polarization tensor provides a common framework.

X.W., I. A. Shovkovy, L. Yu, M. Huang, PRD 102, 076010 (2020); X.W., I. Shovkovy, PRD 104, 056017 (2021).

Low-mass dileptons as a magnetic probe

$M \lesssim \sqrt{|eB|}$: enhanced yield; sizable anisotropy for $k_T \gtrsim \sqrt{|eB|}$.

X.W., I. A. Shovkovy, PRD 106, 036014 (2022).

Go beyond the yield and v_2

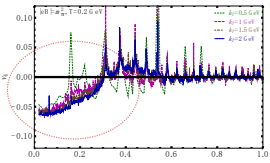
Higher harmonics v_4, v_6 and circular polarization add information about the medium.

X.W., I. A. Shovkovy, PRD 109, 056008 (2024); PRD 110, 116005 (2024).

Our proposal: combine rates, angular anisotropy and polarization as probes.

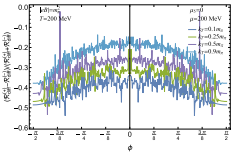
From anisotropy to polarization

Dilepton harmonics

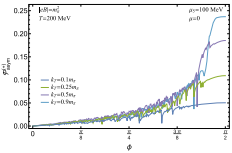


$T = 0.2$ GeV, $|eB| = m_\pi^2$.

Circular photon response



$\mu = 200$ MeV, $\mu_5 = 0$: polarization imbalance.



$\mu = 0$, $\mu_5 = 100$ MeV: directional asymmetry.

$T = 200$ MeV, $|eB| = m_\pi^2$.

Earlier work

- Rates and v_n: energy and direction of the emitted radiation.
- Circular photons: different responses to electric and chiral charge densities.

This talk

- Thermal dileptons: longitudinal/transverse response through decay angles, λ_θ.
- ϕ/K^{*0}: flavor dependence of pole occupation and current spectral response.

X.W., I. A. Shovkovy, PRD 109, 056008 (2024); PRD 110, 116005 (2024).

v_n: emission azimuth λ_θ: dilepton decay angle.

Spin alignment and polarization

The decay analyzers differ.

Vector meson → two pseudoscalars

$$\frac{1}{N}\frac{dN}{d\cos\theta^*} = \frac{3}{4}\Big[(1-\rho_{00}) + (3\rho_{00}-1)\cos^2\theta^*\Big].$$

$\rho_{00} = P(m=0)$ along the chosen axis.
For unpolarized mesons, $\rho_{00} = 1/3$.
Tensor alignment can be nonzero even if $\langle \boldsymbol{S} \rangle = 0$.

Virtual photon → $\ell^+\ell^-$

$$\frac{dR}{d\Omega_\ell} \propto 1 + \lambda_\theta \cos^2\theta_\ell + \cdots$$

For unpolarized photons, $\lambda_\theta = 0$.
$\lambda_\theta = +1$ for transverse polarization and
$\lambda_\theta = -1$ for longitudinal polarization ($m_\ell = 0$).

Polar-angle dependence after integration over azimuth

Parent polarization	$V \to PP$	$\gamma^* \to \ell^+\ell^-$ $(m_\ell = 0)$
Longitudinal ($m = 0$)	$\cos^2\theta$	$\sin^2\theta$
Transverse ($m = \pm 1$)	$\sin^2\theta$	$1 + \cos^2\theta$

Polarization decomposition

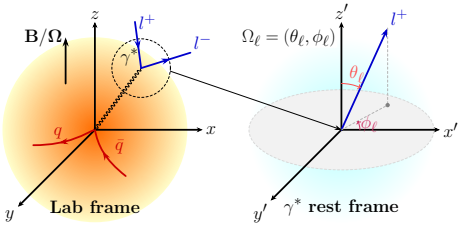
$$\mathcal{S}_{\lambda\lambda'}(q) = \epsilon^*_\mu(\lambda)\,\mathcal{A}^{\mu\nu}(q;T,B)\,\epsilon_\nu(\lambda'), \qquad \lambda = 0, +, -.$$

Channel	Microscopic object	Projection used here
Electromagnetic	$J^\mu_{\rm em} = \sum_f Q_f \bar{q}_f \gamma^\mu q_f$	Dilepton angular distribution
NJL mesons	$j^\mu_\phi = \bar{s}\gamma^\mu s$, $j^\mu_K = \bar{s}\gamma^\mu d$	Pole occupation / current ratio

Common tensor structure; distinct operators and spectral weights.

$\mathcal{A}$ is generic notation; each model retains its own normalization.

Landau quantization



Uniform field: $\boldsymbol{B} = B\hat{\boldsymbol{z}}$

$$E_{n,f}^2 = p_z^2 + m_f^2 + 2n|q_f B|.$$

Longitudinal and transverse currents access different Landau transitions. Pair creation and thermal transitions introduce distinct thresholds.

For the magnetized numerical results, $\boldsymbol{q} = 0$ and the spin axis is $\hat{\boldsymbol{B}}$.

The general geometry uses a moving photon; at $\boldsymbol{q} = 0$ the helicity direction is undefined, so the field axis is specified explicitly.

Physics processes

$$m_{n,f} = \sqrt{m_f^2 + 2n|q_f B|}, \qquad E_{n,f}(p_z) = \sqrt{p_z^2 + m_{n,f}^2}, \qquad \boldsymbol{q} = 0.$$

Quark–antiquark annihilation

$$M = E_{n,f}(p_z) + E_{n',f}(p_z),$$
$$M \geq m_{n,f} + m_{n',f}.$$

A pair channel opens above its threshold.

Thermal Landau-level transition

$$M = E_{n,f}(p_z) - E_{n',f}(p_z), \quad n > n',$$
$$0 < M \leq m_{n,f} - m_{n',f}.$$

A thermally occupied parton emits a virtual photon while dropping to a lower level.

Selection rules at $q = 0$: $J_\parallel$: $\Delta n = 0$; $J_\perp$: $|\Delta n| = 1$.

Channel openings change the longitudinal/transverse balance.

Thermal dilepton rate

$$\frac{dR}{d^4q\, d\Omega_\ell} \propto 1 + \lambda_\theta \cos^2\theta_\ell + \lambda_\varphi \sin^2\theta_\ell \cos 2\varphi_\ell + \lambda_{\theta\varphi} \sin 2\theta_\ell \cos\varphi_\ell + \cdots$$

For a pair at rest in our charge-symmetric medium,

$$\mathcal{A}^{ij} \propto M\, \mathrm{diag}(\sigma_\perp, \sigma_\perp, \sigma_\parallel).$$

Angle-integrated rate

$$\frac{dR}{d^4q} \propto \frac{n_B(M)}{M}(2\sigma_\perp + \sigma_\parallel).$$

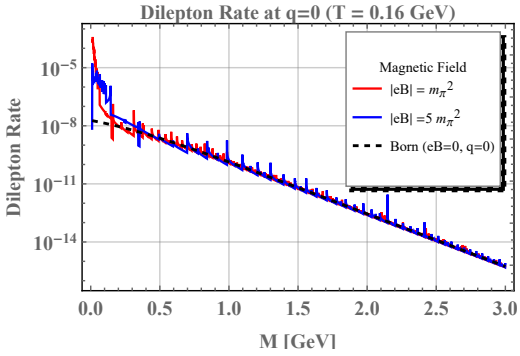
Measures the sum of spin channels.

Polar anisotropy

$$\lambda_\theta = \frac{\sigma_\perp - \sigma_\parallel}{\sigma_\perp + \sigma_\parallel}.$$

Measures their relative imbalance.

Dilepton production rate

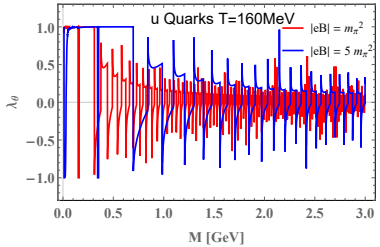


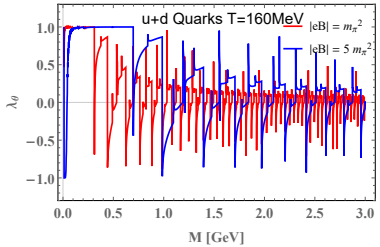
$T = 160$ **MeV,** $q = 0$

- $m_u = m_d = 5$ MeV.
- $|eB| = m_\pi^2$ and $5m_\pi^2$.
- Enhancement at low mass: $M \lesssim 0.6$ GeV.
- Closer to the Born rate at larger M.

X.W., I. A. Shovkovy, PRD 106, 036014 (2022); H. He, B. Hou, X.W. and M. Wei, arXiv:2607.11634.

Polarization: mass dependence





u-quark contribution

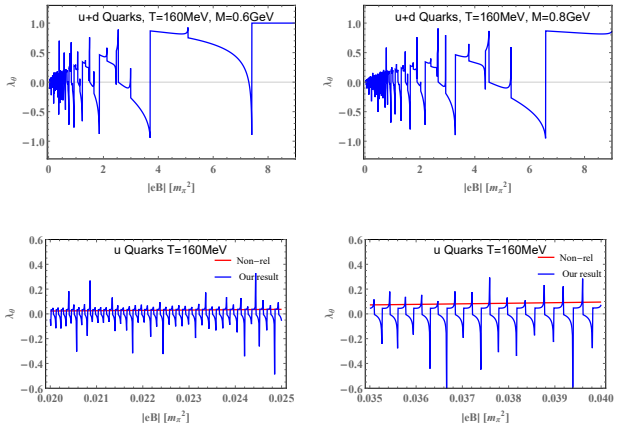
Longitudinal and transverse channels open at different Landau-level thresholds, producing sharp changes in $\lambda_\theta(M)$.

Combined $u + d$ contribution

The oscillations persist when both flavors contribute, even at masses where the dilepton rate approaches the Born rate.

$T = 160$ MeV, $\boldsymbol{q} = 0$.
$|eB|/m_\pi^2 = 1$ (red), 5 (blue).

A larger pair mass shifts the polarization dips to stronger fields



The first excited longitudinal channel

As the $n = 1$ threshold $2\sqrt{m_f^2 + 2|q_f B|}$ approaches M from below, longitudinal strength drives λ_θ down.

At $M = 0.6$ GeV the u and d dips lie near 3.7 and 7.4 m_π^2. At 0.8 GeV the u dip moves to 6.6 m_π^2.

Weak-field detail at $M = 0.6$ GeV

The blue oscillations are more closely spaced in the left panel.

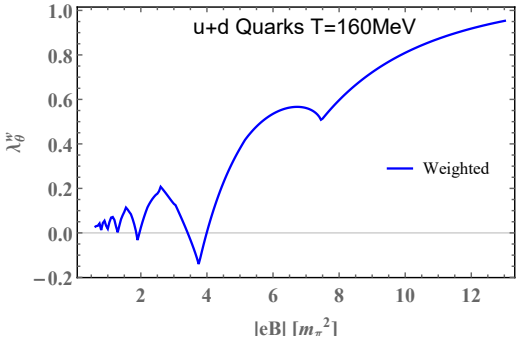
Nonrelativistic coalescence gives

$$\rho_{00}^{\mathrm{NR}} \simeq \frac{1}{3} - \frac{q_f q_{f'} B^2}{9T^2 M_f M_{f'}}.$$

Opposite charges imply $\lambda_\theta^{\mathrm{NR}} < 0$. The red reference is positive as plotted.

Coalescence: Y.-G. Yang, R.-H. Fang, Q. Wang, X.-N. Wang, PRC 97, 034917 (2018).

Dilepton polarization averaged over invariant mass



Yield weighting over 0.6–3.0 GeV

$$\lambda_\theta^w = \frac{\int dM\, R(M)\lambda_\theta(M)}{\int dM\, R(M)}, \qquad R(M) = \frac{dR}{dM}.$$

The thermal yield gives more weight to pairs at the lower end of the mass window.

Magnetic-field dependence

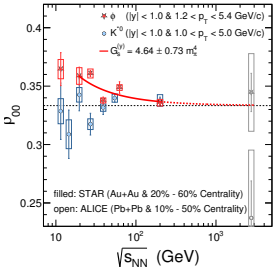
A dip remains near $|eB| = 3.8\, m_\pi^2$. At the strongest fields shown, λ_θ^w approaches +1.

Spin alignment at RHIC and LHC

$\rho_{00} = 1/3$ is the isotropic reference along the event-plane normal.

RHIC / STAR

Au+Au, 20–60%, $|y| < 1$



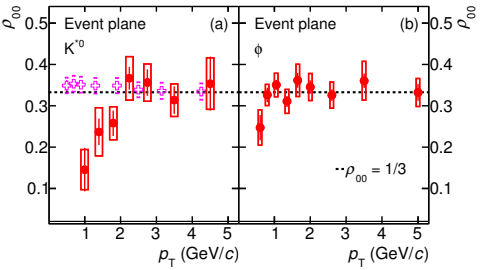
ϕ: BES energy average above 1/3.

K^{*0}: consistent with 1/3.

STAR Collaboration, Nature 614, 244 (2023).

LHC / ALICE

Pb–Pb, 2.76 TeV, 10–50%, $|y| < 0.5$



Both central values fall below 1/3 at low p_T.

Higher p_T: consistent with 1/3.

ALICE Collaboration, PRL 125, 012301 (2020).

ϕ and K^{*0} in the NJL model

Sheng et al. studied magnetic mass splitting and spin alignment of the ϕ in the NJL model.

X.-L. Sheng, S.-Y. Yang, Y.-L. Zou and D. Hou, Eur. Phys. J. C **84**, 299 (2024).

Our comparison of ϕ and K^{*0}

$$\phi = s\bar{s}, \quad K^{*0} = d\bar{s}, \quad q_d = q_s = -e/3.$$

Both channels use $b = |eB|/3$ and the same couplings, with $(a, b) = (s, s)$ or (d, s).

$$M_f = m_f - 4G_S\sigma_f + 2K\sigma_g\sigma_h.$$

Uniform B, $\mu = 0$, $\boldsymbol{q} = 0$.

Spin projection and RPA propagator

$$J_{V,\lambda}(w) = e_\lambda^{i*}\, J_{ab}^{ik}(w)\, e_\lambda^k.$$

$e_0 \parallel \boldsymbol{B}$ and $e_\pm = (\hat{x} \pm i\hat{y})/\sqrt{2}$ for $\boldsymbol{B} \parallel \hat{z}$.

$$D_{V,\lambda}(w) = \frac{g}{1 - gJ_{V,\lambda}(w)}, \qquad g = 4|G_V|.$$

The pole satisfies $1 - gJ_{V,\lambda}(M_{V,\lambda}) = 0$.

One-loop polarization tensor

$$J_{ab}^{ik}(i\nu_\ell) = -N_c T \sum_r \int \frac{d^3p}{(2\pi)^3}\, \mathrm{tr}_D\left[\gamma^i \widehat{S}_a(i\omega_r, \boldsymbol{p})\, \gamma^k \widehat{S}_b(i\omega_r + i\nu_\ell, \boldsymbol{p})\right].$$

We sum all Landau levels, apply Pauli–Villars regularization and continue $i\nu_\ell \to w = \omega + i0^+$.

X.W., Z. Ouyang, M. Wei, in preparation.

Spin-dependent pair thresholds

At $q = 0$, with $b = |eB|/3$

$$\omega_{\mathrm{th},0} = M_d + M_s,$$

$$\omega_{\mathrm{th},+} = \sqrt{M_d^2 + 2b} + M_s, \qquad \omega_{\mathrm{th},-} = M_d + \sqrt{M_s^2 + 2b}.$$

Longitudinal polarization couples equal Landau levels. The two circular components raise the level on different flavor lines.

For ϕ, equal constituent masses restore circular degeneracy.

For K^{*0}, unequal masses distinguish the thresholds; reversing B exchanges the circular labels.

The threshold fixes the start of a cut; the resummed interaction fixes the pole.

Two definitions of spin response

Conditional isolated-pole occupation

$$\rho_{00}^{\mathrm{qp}} = \frac{n_B(M_0)}{\sum_{\lambda=0,+,-} n_B(M_\lambda)}.$$

An occupation of isolated, positive-residue real poles in the zero-width equilibrium limit. Depends on pole energies; current residues have been divided out.

Pole-plus-pair current ratio

$$R_{00}^{\mathrm{cur}} = \frac{I_0}{I_0 + I_+ + I_-}, \qquad I_\lambda = I_\lambda^b + I_\lambda^c,$$

$$I_\lambda^b = Z_\lambda n_B(M_\lambda), \qquad Z_\lambda^{-1} = \left.\frac{\partial J_{V,\lambda}}{\partial w^2}\right|_{w^2=M_\lambda^2}.$$

Z_λ is the isolated pole's weight in spin channel λ.

$$I_\lambda^c = \int_{\omega_{\mathrm{th},\lambda}}^{5\,\mathrm{GeV}} d\omega\, 2\omega n_B(\omega)\xi_\lambda(\omega).$$

$\xi_\lambda(\omega) = \frac{1}{\pi}\,\mathrm{Im}\, D_{V,\lambda}(\omega + i0^+)$ is the meson spectral density for spin projection λ. I_λ^c samples its quark–antiquark continuum.

Neither construction is automatically the reconstructed meson ρ_{00}.

Magnetic mass splitting

Mean transverse–longitudinal gap

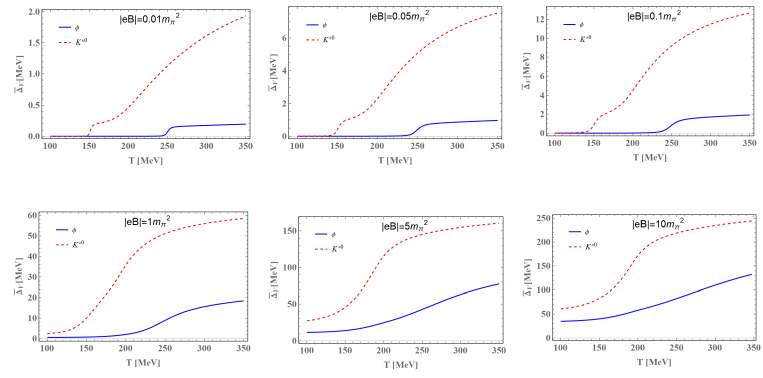
$$\bar{\Delta}_V \equiv \Delta_V = \frac{M_{V,+} + M_{V,-}}{2} - M_{V,0}$$

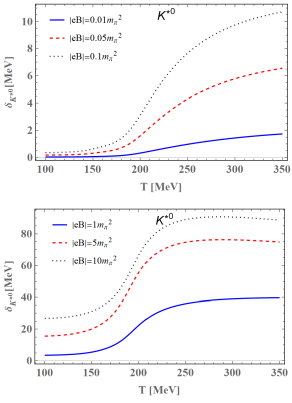
Solid ϕ and dashed K^{*0} at fixed field.

Circular half-splitting

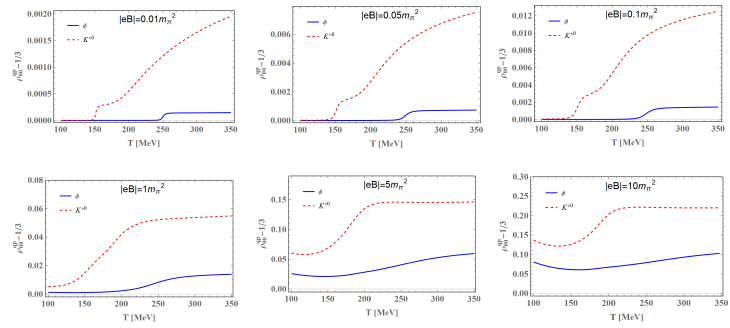
$$\delta_V = \frac{M_{V,+} - M_{V,-}}{2},\ \delta_\phi = 0$$

K^{*0} splits for $M_d \neq M_s$.





Spin alignment: isolated poles



Each panel shows $\rho_{00}^{\mathrm{qp}} - 1/3$ versus T at fixed $|eB|$.

K^{*0} remains above ϕ at all six field strengths.

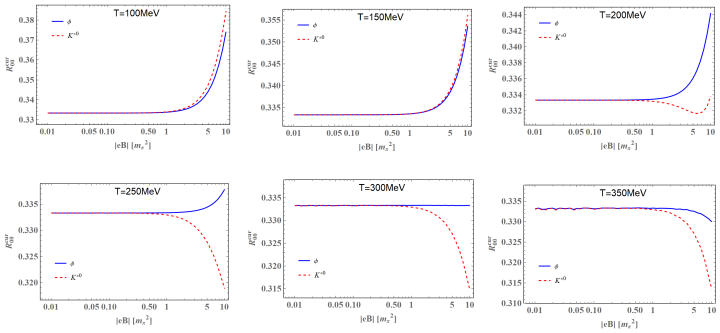
In the dilute limit $\left(n_B(M) \approx e^{-M/T}\right)$,

$$\rho_{00}^{\mathrm{qp}} \simeq \frac{1}{1+2\chi_V},$$

$$\chi_V = e^{-\Delta_V/T}\cosh(\delta_V/T).$$

This result is conditional on the pole construction.

Spin response: current spectra



Weak fields: close to $1/3$.
For $2.5 \leq eB/m_\pi^2 \leq 10$:

- At 100–150 MeV, both channels increase.
- At 200 MeV, K^{*0} is nonmonotonic.
- At 250–350 MeV, K^{*0} decreases.

ϕ is almost field independent at 300 MeV in this range.

ϕ versus K^{*0}

$T = 200$ MeV, $\quad eB = 5m_\pi^2$

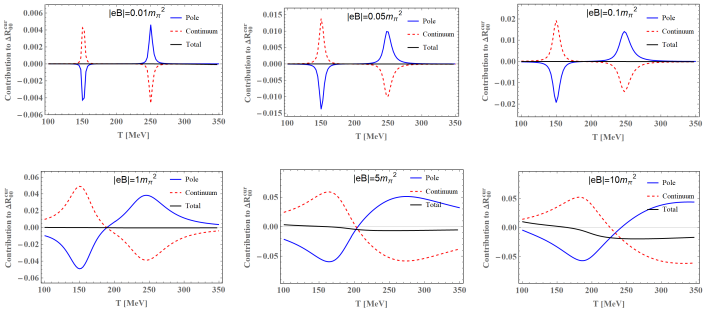
Quantity	ϕ	K^{*0}	Ordering
Conditional pole occupation ρ_{00}^{qp}	0.36174	0.46849	$K^{*0} > \phi$
Current spectral ratio R_{00}^{cur}	0.33610	0.33176	$K^{*0} < \phi$

Larger magnetic mass splitting does not imply a larger current ratio.

At $eB/m_\pi^2 = 1, 5, 10$, the current ordering changes between 150 and 200 MeV.

Pole and continuum contributions

$$R_{00}^{\mathrm{cur}} - \frac{1}{3} = \frac{I_0^b - S^b/3}{S} + \frac{I_0^c - S^c/3}{S}, \qquad S^{b,c} = \sum_\lambda I_\lambda^{b,c}, \quad S = S^b + S^c.$$



The pole and continuum terms in ΔR can largely cancel.

At $eB = 5m_\pi^2, T : 150 \to 200$ MeV:

$$f_K : 0.69 \to 0.20,$$
$$f_\phi : 0.92 \to 0.77,$$

with $f_V = S_V^b / S_V$.

Contributions to $\Delta R = R_K^{\mathrm{cur}} - R_\phi^{\mathrm{cur}}$ at six fixed field strengths. Blue solid: pole. Red dashed: continuum. Black solid: total.

Summary

Thermal dileptons

Low-mass pairs favor transverse polarization. As M increases, successive Landau levels open in different spin channels, and $\lambda_\theta(M)$ oscillates with decreasing amplitude.

Weighting by the dilepton yield smooths the oscillations and leaves an overall preference for transverse polarization at strong fields.

ϕ and K^{*0} in the NJL model

K^{*0} has a larger transverse–longitudinal mass gap than ϕ. Its two circular modes split, while those of ϕ remain degenerate. Across the temperatures studied, a stronger field favors longitudinal pole occupation in both mesons, more strongly in K^{*0}.

Both current ratios stay near $1/3$ in weak fields. At stronger fields, the K^{*0} ratio crosses from above the ϕ ratio to below it as T rises. Pole residues and the growing K^{*0} pair continuum account for this reversal.

Thank you!